Ocean Engineering 313 (2024) 119458

Contents lists available at ScienceDirect

Ocean Engineering

journal homepage: www.elsevier.com/locate/oceaneng

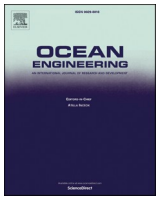

Research paper

Bayesian finite element model inversion of offshore wind turbine structures for joint parameter-load estimation

Mohammad Valikhani [a], Mansureh Nabiyan [b], Mingming Song [c], Vahid Jahangiri [d], Hamed Ebrahimian [a,*], Babak Moaveni [e]

[a] Dept. of Civil and Environmental Engineering, University of Nevada, Reno, NV, United States
[b] Venterra Group (Gavin & Doherty Geosolutions Ltd.), Dublin, Ireland
[c] Dept. of Bridge Engineering, Tongji University, Shanghai, China
[d] Leeward Renewable Energy LLC, Dallas, TX, United States
[e] Dept. of Civil and Environmental Engineering, Tufts University, Medford, MA, United States

ARTICLE INFO

Keywords:
Offshore wind turbine
Input load estimation
FE model updating
Bayesian inference
Data assimilation

ABSTRACT

Operating in harsh and unsteady marine environment, offshore wind turbine (OWT) structures are exposed to unpredictable wind and wave loads. Identifying the structural loads and their effects on the OWTs allow for predicting the remaining fatigue life of these structures and improving the structural design procedure. In this paper, a finite element (FE) model inversion method is presented to estimate the unknown loads and model parameters of OWTs using sparse measurement data. A realistic FE model of an OWT structure with jacket substructure is created in the open-source simulation platform, OpenSees. A Bayesian inference framework is presented to integrate the measured data with the FE model to estimate unknown wind loads and mass of rotor-nacelle assembly. To evaluate the performance of this data assimilation framework, the effect of sensor type, number of sensors, and modeling errors on the estimation accuracy of wind loads and model parameters are investigated through different case studies where synthetic data are used as measurements. The results of this study are important to guide instrumentation of new OWT structures, and to understand the potential limitations and sources of error in the real-world application of this data assimilation framework for joint model parameter and input load estimation.

1. Introduction

Offshore wind turbine (OWT) structures operate in harsh marine environment and are exposed to unpredictable dynamic loads (Röckmann et al., 2017). Dynamic loads impact the remaining useful life and can result in fatigue failure in OWT components and structure (Igwemezie et al., 2019). Because of the uncertain operational conditions, loadings considered in the design stage of OWT structures can be different from the operational stage, so fatigue life can be shorter than what is expected. Estimation of the wind and wave loads from the dynamic response of the structure can improve the fatigue design process and can be further used to predict the remaining useful life of structures for instrumented OWTs. Additionally, any potential damage or deterioration in the structural system can be identified by tracking the structural properties such as mass and stiffness. In this paper, a finite element (FE) model updating method is presented for estimating structural model parameters and unknown loads of an OWT using sparsely measured structural responses. The objective is to evaluate the efficacy of the method and understand its potential and limitations for real-world application through a series of case studies using numerically simulated data.

In the FE model updating process, mechanics-based laws are employed to develop a structural model, and measurement responses are used to estimate the unknown model parameters and input loads. Two main approaches exist for FE model updating: frequency-domain model updating (Augustyn et al., 2020; Friswell and Mottershead, 1995; Hu et al., 2018) and time-domain model updating (Ebrahimian et al., 2015; Eftekhar Azam et al., 2015; Naets et al., 2015). In the frequency-domain model updating, first, the numerical model of the structure is parametrized based on the structural parameters such as stiffness, damping, and mass. Through experimental modal analysis or operation modal analysis (OMA), modal properties are identified using measurement data. Then,

* Corresponding author.
E-mail address: hebrahimian@unr.edu (H. Ebrahimian).

https://doi.org/10.1016/j.oceaneng.2024.119458
Received 14 June 2024; Received in revised form 24 September 2024; Accepted 5 October 2024
Available online 24 October 2024

model parameters are estimated by minimizing the discrepancies between model-predicted and identified modal properties. Conventional OMA methods have been used for wind turbine structural health monitoring, condition assessment, and modal identification (Augustyn et al., 2020; Devriendt et al., 2014; Hines et al., 2023; Moynihan et al., 2023; Ozbek and Rixen, 2013; Song et al., 2022, 2023; Xu et al., 2020). These methods include natural excitation technique combined with eigensystem realization algorithm (NExT-ERA) (James III et al., 1993) and data-driven stochastic subspace identification (SSI) (Oliveira et al., 2016; Peeters and de Roeck, 1999), which are based on the broadband assumption for input excitations. Nevertheless, because of the rotation of turbine blades, the excitation frequencies would include harmonic components, such as fundamental rotational (1 P) and blade passing frequencies (3 P for three-bladed turbines) (Van der Tempel, 2006), which may affect the modal identification accuracy. Various modified OMA approaches have been developed to deal with the disturbing harmonic components of structural responses to improve modal identification accuracy (Dai et al., 2017; Jacobsen et al., 2007; Pintelon et al., 2010). Using classical OMA at idling or parked conditions can also minimize the effect of harmonic components in the modal identification of wind turbines (Augustyn et al., 2020; Devriendt et al., 2014). In this paper, we pursue a time-domain model updating approach to avoid the potential shortcomings of frequency-domain methods.

Time-domain model updating approaches can be used to estimate jointly the states, model parameters, and input forces of a dynamic system (Naets et al., 2015). In these approaches, the state of the system is augmented with unknown model parameters and inputs, and an Extended Kalman filter (EKF) (Simon, 2006) can be employed to estimate the augmented state. Fallais et al. (2016) identified the hydrodynamic load and stiffness of an OWT with an EKF using simulated data. Maes et al. (2016) compared three algorithms, including Kalman filter, a joint input-state estimation, and modal expansion, to monitor the dynamic strains in the OWT tower with monopile substructure at parked and operating conditions. All three algorithms were evaluated for a given model of the structure and compared when acceleration-only data or a combination of acceleration and strain data were used. For acceleration-only data, joint input-state estimation and modal expansion provided acceptable results, while the inclusion of strain data improved the KF-based results. Nabiyan et al. (2021) employed a sequential Bayesian inference method to estimate an unknown model parameter (rotational stiffness of the foundation) jointly with the effective wind load time history applied to a monopile OWT using strain response measurements. They compared the accuracy of this estimation method with the modal expansion method for predicting flexural moment time history at the mudline. The results show that the Bayesian algorithm can be more accurate than the modal expansion method. Song et al. (2022) used a recursive Bayesian inference approach for joint parameter-input estimation and strain time history prediction of an offshore platform in the North Sea. They updated the FE model of the structure using acceleration and strain data and compared their proposed method with the modal expansion-based method for strain prediction. They observed that the Bayesian framework provides more accurate strain prediction than the modal expansion method. The Bayesian inference also has been employed for monitoring monopile of OWT (Xu et al., 2023), virtual modeling of offshore jacket structures (Wang et al., 2022), optimal sensor placement (Mehrjoo et al., 2022), load identification of wind turbines (Wei et al., 2023), support condition monitoring of OWT (Ren et al., 2023), fatigue monitoring of wind turbines (Flores Terrazas et al., 2022), breaking wave load estimation (Maes et al., 2018), virtual sensing of subsoil strain response (Zou et al., 2023), foundation parameter estimation of OWT (Simpson et al., 2024), and fatigue stress assessment of OWT (Noppe et al., 2018; Tatsis et al., 2017).

In the previous studies, OWT model updating has been carried out based on simplified structural models (Dai et al., 2017; Fallais et al., 2016; Xu et al., 2020), white noise assumption for input excitation (Oliveira et al., 2016), and non-operational conditions, i.e., idling or parked (Augustyn et al., 2020; Devriendt et al., 2014). Past studies considered a simple 2D model of the structure and estimated the input wind force only in one direction (Dai et al., 2017; Fallais et al., 2016; Xu et al., 2020); while in an actual OWT, the wind and wave loads excite the structure in both side-to-side and fore-aft directions simultaneously.

This study is a proof-of-concept for creating virtual models of wind turbine structures (digital twinning) and predicting the responses at inaccessible locations (virtual sensing). The aim is to investigate the application and limitation of time-domain model updating for joint parameter-load estimation in OWTs. For this purpose, the study is based on synthetic data to provide an upper bound accuracy on the estimation results. Realistic model of a jacket-based OWT, which represents the turbines at Block Island Wind Farm (BIWF) in the United States, under realistic loadings is built to generate synthetic data recorded from realistic sensor configurations.

In this paper, a window-based Bayesian model updating of jacket-based OWT model is developed through a 3D FE model. Simulated responses of the OWT structure under wind and wave loads are used to estimate jointly the unknown model parameters and wind loads applied to the tower at both side-to-side and fore-aft directions. The model updating method is implemented in the time domain and can be used at any operational condition of OWTs without any assumptions about the input loads. The window-based Bayesian model updating was first developed by Ebrahimian et al. (2018) and has been applied to model updating of civil structures (Ghahari et al., 2020), digital twinning of a bridge (Ghahari et al., 2022), virtual sensing of a wind turbine (Nabiyan et al., 2021), and model inversion of wind turbine drivetrain (Valikhani et al., 2023). Here, this method is applied to an OWT under simulated wave and wind loads at both side-to-side and fore-aft directions. The simulated loads are extracted from OpenFAST (NREL, 2022) and imported to the 3D FE model of the OWT. The 3D FE model is created in OpenSees platform (McKenna et al., 2000) to simulate structural responses. Acceleration responses at three locations of the tower structure, and strain responses at the base and middle level of the tower are simulated, contaminated with white noise, and considered as measurement data for model updating. Then, given the model and measurement data, the wind loads at the top of tower including forces and moments in both side-to-side and fore-aft directions are estimated in conjunction with mass of rotor-nacelle assembly (RNA). The effects of sensor type, number of sensors, and modeling error on the estimated model parameters and wind input loads are investigated through different case studies.

2. Estimation and modeling procedures

2.1. Bayesian model updating

Bayesian model updating is used to simultaneously estimate unknown model parameters and wind loads of an OWT structure. To apply the Bayesian framework, we assume that the finite element model is accurate without any modeling error, with the uncertainty stemming from unknown model parameters and loads, which are augmented to a parameter vector. The parameter vector is modeled as random variables with a joint prior Gaussian probability density function (PDF). Moreover, an observation model is assumed to be a Gaussian white noise process. Under the Gaussian assumption for the prior PDF of the parameter vector and the likelihood function, the posterior PDF of the parameter vector conditioned on observation data can be updated.

The time-discretized equation of motion of a linear FE model of a dynamical system at time step t can be written as

$$\mathbf{M}(\boldsymbol{\theta})\ddot{\mathbf{x}}_t + \mathbf{C}(\boldsymbol{\theta})\dot{\mathbf{x}}_t + \mathbf{K}(\boldsymbol{\theta})\mathbf{x}_t = \mathbf{u}_t^* \tag{1}$$

in which $\boldsymbol{\theta} \in \mathbb{R}^{n_\theta \times 1}$ is model parameter vector, where n_θ denotes the number of unknown model parameters, $\mathbf{M}(\boldsymbol{\theta}), \mathbf{C}(\boldsymbol{\theta}), \mathbf{K}(\boldsymbol{\theta}) \in \mathbb{R}^{n_{\mathrm{DOF}} \times n_{\mathrm{DOF}}}$ are

parameterized mass, damping, and stiffness matrices, respectively, where n_{DOF} denotes the number of degrees of freedom. $\ddot{\mathbf{x}}_t$, $\dot{\mathbf{x}}_t$, $\mathbf{x}_t$, $\mathbf{u}_t^* \in \mathbb{R}^{n_{\text{DOF}}\times 1}$ denote acceleration, velocity, displacement, and input load (i.e., wind and wave loads in this study) vectors, respectively. The subscript t denotes the time step such that $t = 1,2,\cdots,T$, where T indicates the total number of time steps.

Eq. (1) can be solved recursively in time, for example by the Newmark-beta time integration method (Chopra, 2007). In general, the response of the structural model at time step t can be expressed as a nonlinear function of the unknown model parameters $\boldsymbol{\theta}$, the input load vector time history from time step 1 to time step t, and initial velocity and displacement vectors as

$$\hat{\mathbf{y}}_t = \mathbf{h}_t\left(\boldsymbol{\theta}, \mathbf{u}_{1:t}^*, \dot{\mathbf{x}}_0, \mathbf{x}_0\right) \tag{2}$$

in which $\mathbf{u}_{1:t}^* = \left[\mathbf{u}_1^{*T}, \mathbf{u}_2^{*T}, \cdots, \mathbf{u}_t^{*T}\right]^T$ represents the time history of the input load vector; $\dot{\mathbf{x}}_0$ and $\mathbf{x}_0 \in \mathbb{R}^{n_{\text{DOF}}\times 1}$ denote initial velocity and displacement vectors; and $\mathbf{h}_t(.) \in \mathbb{R}^{n_{\text{y}}\times 1}$ is the nonlinear response function of the FE model at time step t, where n_{y} denotes the number of measured responses.

A measurement model can be expressed in the terms of predicted response and measurement noise at time step t as

$$\mathbf{y}_t = \hat{\mathbf{y}}_t + \mathbf{v}_t \quad \mathbf{v}_t \sim N(\mathbf{0}, \mathbf{R}_k) \tag{3}$$

where $\mathbf{y}_t \in \mathbb{R}^{n_{\text{y}}\times 1}$ denotes measured response vector, $\hat{\mathbf{y}}_t \in \mathbb{R}^{n_{\text{y}}\times 1}$ denotes the model-predicted response vector given in Eq. (2), and $\mathbf{v}_t \in \mathbb{R}^{n_{\text{y}}\times 1}$ represents the measurement noise vector, which is assumed to be a Gaussian white noise process with zero mean and covariance matrix of $\mathbf{R}_t \in \mathbb{R}^{n_{\text{y}}\times n_{\text{y}}}$.

In the FE model expressed by Eq. (2), the model parameters and some input loads are unknown (wind loads in this study), and a window-based Bayesian inference approach (Ebrahimian et al., 2018) is adopted to estimate them using measurement data. In this approach, the measurement dataset is divided into overlapping windows referred to as the estimation windows. Considering the m^{th} estimation window with the starting time t_1^m and ending time t_2^m as shown in Fig. 1, the window length is $t_l = t_2^m - t_1^m$. The measurement dataset at this window can be represented by $\mathbf{y}_{t_1^m:t_2^m} = \left[\mathbf{y}_{t_1^m}^T, \mathbf{y}_{t_1^m+1}^T, \cdots, \mathbf{y}_{t_2^m}^T\right]^T$, which includes all measurements in the time interval t_1^m to t_2^m. Assume that the estimation window m has t_o overlapping time steps with the next window $m+1$, so the sliding stride, which is defined as the time step difference between starting times of two successive windows equals to $t_s = t_l - t_o$.

In the window-based Bayesian inference method, the aim is to obtain the maximum a posteriori estimate of the updating parameters given the measurement dataset at the estimation window m, i.e., $max_{\boldsymbol{\varphi}_m} p\left(\boldsymbol{\varphi}_m | \mathbf{y}_{t_1^m:t_2^m}\right)$, where the parameter vector $\boldsymbol{\varphi}_m$ includes unknown model parameters, $\boldsymbol{\theta}$, and time history of unknown input load vector, $\mathbf{u}_{t_1^m:t_2^m}$, across the m^{th} estimation window, i.e., $\boldsymbol{\varphi}_m = \left[\boldsymbol{\theta}^T \quad \mathbf{u}_{t_1^m:t_2^m}^T\right]^T$. The updated model parameter vector is then transferred to the next estimation window as initial values. A brief review of the method is provided next.

The posterior PDF of the parameter vector $\boldsymbol{\varphi}_m$ given the measurement $\mathbf{y}_{t_1^m:t_2^m}$ can be determined through the Bayes' theorem as (Ebrahimian et al., 2018)

$$p\left(\boldsymbol{\varphi}_m | \mathbf{y}_{t_1^m:t_2^m}\right) = \frac{p\left(\mathbf{y}_{t_1^m:t_2^m} | \boldsymbol{\varphi}_m\right) p(\boldsymbol{\varphi}_m)}{p\left(\mathbf{y}_{t_1^m:t_2^m}\right)} \tag{4}$$

where $p\left(\mathbf{y}_{t_1^m:t_2^m} | \boldsymbol{\varphi}_m\right)$ and $p(\boldsymbol{\varphi}_m)$ denote the likelihood function and the prior PDF of the parameter vector, respectively. The term $p\left(\mathbf{y}_{t_1^m:t_2^m}\right)$ is a normalizing constant.

According to Eq. (3) and assuming that the measurement noise is an independent Gaussian white noise process, the likelihood function $p\left(\mathbf{y}_{t_1^m:t_2^m} | \boldsymbol{\varphi}_m\right)$ is a Gaussian distribution with mean $\hat{\mathbf{y}}_{t_1^m:t_2^m}$ (predicted response) and covariance matrix $\tilde{\mathbf{R}} = diag\left(\mathbf{R}_{t_1^m}, \mathbf{R}_{t_1^m+1}, \cdots, \mathbf{R}_{t_2^m}\right)$, where $\mathbf{R}_t$ for $k \in \{t_1^m, \cdots, t_2^m\}$ is the measurement noise covariance matrix at time step k, and is assumed to be time-independent, i.e. $\mathbf{R}_t = \mathbf{R}$, and $diag(\cdot)$ is an operator that gets matrices and forms a block-diagonal matrix. The prior PDF of the parameter vector $p(\boldsymbol{\varphi}_m)$ is assumed to have a Gaussian distribution with mean $\hat{\boldsymbol{\varphi}}_m^-$ and covariance matrix $\left(\hat{\mathbf{P}}_\varphi^-\right)_m$. Under these assumptions and approximating the posterior PDF as Gaussian distribution (Gaussianization), the MAP estimate of the parameter vector, and covariance matrix of posterior PDF can be derived as (Ebrahimian et al., 2018)

$$\begin{aligned} \hat{\boldsymbol{\varphi}}_m^+ &= \hat{\boldsymbol{\varphi}}_m^- + \mathbf{G}\left(\mathbf{y}_{t_1^m:t_2^m} - \hat{\mathbf{y}}_{t_1^m:t_2^m}\right) \\ \left(\hat{\mathbf{P}}_\varphi^+\right)_m &= (\mathbf{I} - \mathbf{GC})\left(\hat{\mathbf{P}}_\varphi^-\right)_m (\mathbf{I} - \mathbf{GC})^T + \mathbf{G}\tilde{\mathbf{R}}\,\mathbf{G}^T \end{aligned} \tag{5}$$

where $\hat{\boldsymbol{\varphi}}_m^+$ and $\left(\hat{\mathbf{P}}_\varphi^+\right)_m$ are the posterior mean vector and covariance matrix of the parameter vector; $\mathbf{G} = \left(\mathbf{C}^T\tilde{\mathbf{R}}^{-1}\mathbf{C} + \left(\hat{\mathbf{P}}_\varphi^-\right)_m^{-1}\right)^{-1}\mathbf{C}^T\tilde{\mathbf{R}}^{-1}$ is the Kalman gain matrix (Simon, 2006); $\mathbf{y}_{t_1^m:t_2^m}$ and $\hat{\mathbf{y}}_{t_1^m:t_2^m}$ denote time histories of measured and model-predicted responses at window m, and $\mathbf{C} = \partial\mathbf{h}_{t_1^m:t_2^m}\left(\boldsymbol{\varphi}_m, \hat{\mathbf{u}}_{1:t_1^m-1}, \dot{\mathbf{x}}_0, \mathbf{x}_0\right)/\partial\boldsymbol{\varphi}_m\Big|_{\boldsymbol{\varphi}_m=\hat{\boldsymbol{\varphi}}_m^-}$ denotes the sensitivity matrix, which is the Jacobian of model-predicted responses with respect to the parameter vector $\boldsymbol{\varphi}_m$ at $\hat{\boldsymbol{\varphi}}_m^-$.

Gaussianization of the posterior PDF described above is a nonlinear procedure, and it can be performed through an iterative process. To improve the convergence of the iterative process at each iteration, the parameter vector becomes subjected to a random perturbation as

$$\varphi_{m,i} = \varphi_{m,i-1} + \mathbf{w}_{i-1} \quad \mathbf{w}_{i-1} \sim N(\mathbf{0}, \mathbf{Q}) \tag{6}$$

where $\boldsymbol{\varphi}_{m,i}$ and $\varphi_{m,i-1}$ are the parameter vector at iteration i and $i-1$, respectively, and $\mathbf{w}_{i-1}$ denotes the perturbation term with zero mean and covariance matrix $\mathbf{Q}$. Using Eq. (6), the prior mean vector and covariance matrix of the parameter vector at iteration i can be predicted as

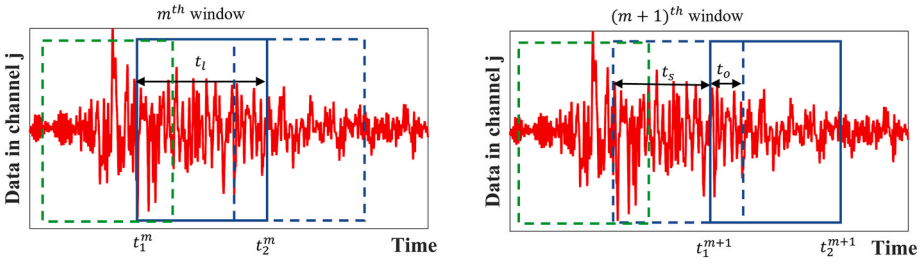

Fig. 1. Dividing the dataset into the overlapping windows in the window-based Bayesian inference approach.

$$\begin{aligned}\widehat{\boldsymbol{\varphi}}_{m,i}^{-} &= \widehat{\boldsymbol{\varphi}}_{m,i-1}^{+} \\ \left(\widehat{\mathbf{P}}_{\varphi}^{-}\right)_{m,i} &= \left(\widehat{\mathbf{P}}_{\varphi}^{+}\right)_{m,i-1} + \mathbf{Q}\end{aligned} \tag{7}$$

where $\widehat{\boldsymbol{\varphi}}_{m,i-1}^{+}$ and $\left(\widehat{\mathbf{P}}_{\varphi}^{+}\right)_{m,i-1}$ are posterior mean vector and covariance matrix at iteration $i-1$ computed using Eq. (5) as $\widehat{\boldsymbol{\varphi}}_{m,i-1}^{+} = \widehat{\boldsymbol{\varphi}}_{m}^{+}$ and $\left(\widehat{\mathbf{P}}_{\varphi}^{+}\right)_{m,i-1} = \left(\widehat{\mathbf{P}}_{\varphi}^{+}\right)_{m}$, and $\widehat{\boldsymbol{\varphi}}_{m,i}^{-}$ and $\left(\widehat{\mathbf{P}}_{\varphi}^{-}\right)_{m,i}$ are prior terms, which are used for updating the mean and covariance matrix in Eq. (5). The iterative process to estimate the parameter vector based on the measurement data at m^{th} estimation window is continued until convergence criteria are satisfied, i.e., the iterative process stops if $\left\|\widehat{\varphi}_{m,i}^{+} - \widehat{\varphi}_{m,i}^{-}\right\| < \epsilon\left\|\widehat{\varphi}_{m,i}^{-}\right\|$ is satisfied, where $\|\cdot\|$ denotes Euclidean norm, and ϵ is the tolerance value. Then, the estimated parameter vector and its associated covariance matrix at the current window are set as initial values for the next estimation window (Ebrahimian et al., 2018). Table 1 summarizes the framework of the window-based Bayesian inference approach for joint input loads and parameter estimation.

2.2. Finite element model of OWT structure

In this paper, we investigate the FE model inversion of an OWT structure, which is located approximately 3 miles southeast of the Block Island in Rhode Island in the United States. The OWT structure consists of a steel tower mounted on a steel jacket structure as shown in Fig. 2. The center of the hub is approximately 100 *m* above the mean sea level (MSL). The substructure consists of a jacket structure with legs connected to piles, a deck, and a transition piece connecting the substructure to the tower. The height of the platform from the MSL is approximately 22 *m*, and the water depth is about 28 *m*.

The FE model of the OWT structure was created in the open-source FE platform, OpenSees (McKenna et al., 2000), to simulate the structure response, and it is interfaced with MATLAB (MathWorks Inc, 2022) for model updating. OpenSees is an object-oriented open-source software for creating linear and nonlinear finite element models of structural and soil systems. The aim of OpenSees is to provide an open-source platform in which researchers can easily build and test their models, and develop new materials, elements, and solvers.

To build the FE model of the OWT structure, the following assumptions are made. The rotor-nacelle-assembly is simplified as a lumped mass on the top of the tower, whose mass and mass moment of inertia are selected based on the actual turbine properties. Only flexural deformation of the tower and jacket are considered, and they are modeled by linear Euler-Bernouli beam elements. The connections of tower bottom and the jacket substructure (transition piece) are modeled using rigid beams constraining rotational and translational degrees of freedom of the nodes at the tower bottom with nodes at the top of the jacket. The boundary conditions of the jacket elements at the mudline are assumed to be fixed.

The FE Model of the OWT structure consists of 61 nodes and 88 elements. The tower is divided into 32 elements along the vertical height to consider changes in the cross-section, see Fig. 3. The substructure is modeled as a frame structure, including 48 elements. The wind loads consist of concentrated forces and moments and are applied to the tower top. The wave loads are distributed over the jacket substructure and are applied as equivalent nodal forces in the finite element model (Bathe, 2006).

The main parameters of the OWT structure for creating the FE model are summarized in Table 2. Some of the parameter values are not disclosed because of confidentiality and reserving the rights of the turbine owner and manufacturer. The RNA mass and moments of inertias are calculated about the local coordinate system, which is described in Section 2.3.1. The jacket and tower element properties including mass, length, cross-section area, and second moment of area are calculated based on the design drawings.

2.3. Wind and wave loads applied on the OWT structure

2.3.1. Wind load

This study uses OpenFAST platform (NREL, 2022) to simulate the wind loads to be applied to the structural model. Wind load can be calculated based on the Blade Element Momentum (BEM) theory, in which a wind turbine blade is divided into small elements acting aerodynamically as a two-dimensional (2D) airfoil (Moriarty and Hansen,

Table 1
A window-based Bayesian inference method for joint input loads and parameter estimation.

1. Setting the window properties and initial values for the first estimation window

1.1 Set the window counter $m = 1$.

1.2 Define the estimation window length t_l and sliding stride t_s.

1.3 Set the initial values of prior mean and covariance matrix of the parameter vector as $\widehat{\boldsymbol{\varphi}}_{m,0}^{+} = \left[\widehat{\boldsymbol{\theta}}_0^T \quad \widehat{\mathbf{u}}_{t_1^1:t_2^1,0}^T\right]^T$, where $\widehat{\boldsymbol{\theta}}_0$ is the initial value of the unknown model parameters and $\widehat{\mathbf{u}}_{t_1^1:t_2^1,0}$ is the initial value of unknown input loads at the first estimation window, and $\left(\widehat{\mathbf{P}}_{\varphi}^{+}\right)_{m,0} = \begin{bmatrix} (\widehat{\mathbf{P}}_{\boldsymbol{\theta}})_0 & \mathbf{0} \\ \mathbf{0} & \left(\widehat{\mathbf{P}}_{\mathbf{u}}^{+}\right)_{t_1^1:t_2^1,0} \end{bmatrix}$, where $(\widehat{\mathbf{P}}_{\boldsymbol{\theta}})_0$ is the prior covariance matrix of the unknown model parameters and $\left(\widehat{\mathbf{P}}_{\mathbf{u}}^{+}\right)_{t_1^1:t_2^1,0}$ is the prior covariance matrix of unknown input loads at the first estimation window.

1.4 Define the perturbation covariance matrix $\mathbf{Q}$ and measurement error covariance matrix $\widetilde{\mathbf{R}}$.

2. Updating the parameter vector and covariance matrix at m^{th} window

2.1 Set the iteration counter $i = 1$.

2.2 Set $\widehat{\varphi}_{m,i}^{-} = \widehat{\varphi}_{m,i-1}^{+}$ and $\left(\widehat{\mathbf{P}}_{\boldsymbol{\varphi}}^{-}\right)_{m,i} = \left(\widehat{\mathbf{P}}_{\boldsymbol{\varphi}}^{+}\right)_{m,i-1} + \mathbf{Q}$.

2.3 Run the model with $\widehat{\boldsymbol{\varphi}}_{m,i}^{-}$ to find the predicted response: $\widehat{\mathbf{y}}_{t_1^m:t_2^m} = \mathbf{h}_{t_1^m:t_2^m}\left(\widehat{\varphi}_{m,i}^{-}, \widehat{\mathbf{u}}_{1:t_1^m-1}, \dot{\mathbf{x}}_0, \mathbf{x}_0\right)$.

2.4 Compute the response sensitivity: $\mathbf{C} = \partial \mathbf{h}_{t_1^m:t_2^m}\left(\boldsymbol{\varphi}_m, \widehat{\mathbf{u}}_{1:t_1^m-1}, \dot{\mathbf{x}}_0, \mathbf{x}_0\right)/\partial \boldsymbol{\varphi}_m\Big|_{\boldsymbol{\varphi}_m = \widehat{\boldsymbol{\varphi}}_{m,i}^{-}}$.

2.5 Compute the Kalman gain matrix: $\mathbf{G} = \left(\mathbf{C}^T\widetilde{\mathbf{R}}^{-1}\mathbf{C} + \left(\widehat{\mathbf{P}}_{\boldsymbol{\varphi}}^{-}\right)_{m,i}^{-1}\right)^{-1}\mathbf{C}^T\widetilde{\mathbf{R}}^{-1}$.

2.6 Compute the parameter vector and associated covariance matrix:
$\widehat{\boldsymbol{\varphi}}_{m,i}^{+} = \widehat{\boldsymbol{\varphi}}_{m,i}^{-} + \mathbf{G}\left(\mathbf{y}_{t_1^m:t_2^m} - \widehat{\mathbf{y}}_{t_1^m:t_2^m}\right)$ and $\left(\widehat{\mathbf{P}}_{\boldsymbol{\varphi}}^{+}\right)_{m,i} = (\mathbf{I} - \mathbf{GC})\left(\widehat{\mathbf{P}}_{\boldsymbol{\varphi}}^{-}\right)_{m,i}(\mathbf{I} - \mathbf{GC})^T + \mathbf{G}\widetilde{\mathbf{R}}\mathbf{G}^T$.

2.7 Check the convergence criteria $\|\widehat{\boldsymbol{\varphi}}_{m,i}^{+} - \widehat{\boldsymbol{\varphi}}_{m,i}^{-}\| < \epsilon\|\widehat{\boldsymbol{\varphi}}_{m,i}^{-}\|$, and if it is satisfied, go to step 3, otherwise, set $i = i+1$ and repeat from step 2.2.

3. Setting the initial values of the parameter vector and covariance matrix for $(m+1)^{th}$ estimation window

3.1 Set $m = m+1$.

3.2 Compute the initial parameter vector: $\widehat{\boldsymbol{\varphi}}_{m,0}^{-}$ (see Ref. (Ebrahimian et al., 2018) for more details).

3.3 Compute the covariance matrix: $\left(\widehat{\mathbf{P}}_{\boldsymbol{\varphi}}^{-}\right)_{m,0}$ (see Ref. (Ebrahimian et al., 2018) for more details).

3.4 Return to Step 2.

Fig. 2. Block Island Wind Farm, in Rhode Island, United States (Photo credit: Gary Norton, DOE).

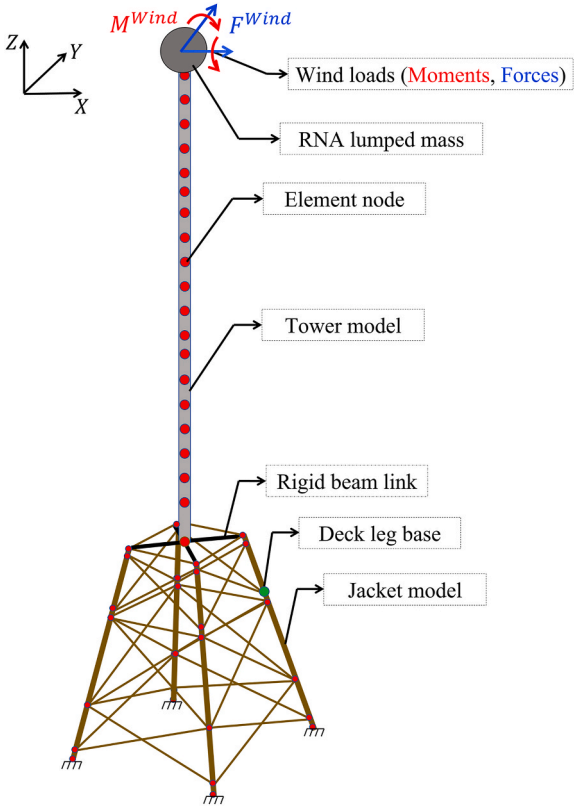

Fig. 3. Schematics of the FE model of the OWT structure.

Table 2
The main parameters of the OWT structure.

Components	Parameters (geometrical and physical)	
	Names	Values
Nacelle	RNA mass	Confidential
	RNA mass moments of inertias	Confidential
Tower	Length	78 m
	Inner and outer radiuses	Confidential
	Moments of area	Confidential
	Modulus of elasticity and Poission's ratio	200 GPa, and 0.25
	Density	7850 Kg/m^3
Deck and jacket (including legs and braces)	All geometrical parameters	Confidential
	Modulus of elasticity and Poission's ratio	200 GPa, and 0.25
	Density	7850 Kg/m^3

2005). In this paper, the turbulence wind regime is considered, and Kaimal spectrum (Jonkman and Buhl, 2005) is selected to determine the turbulence component of the wind velocity as

$$S_v(f) = \frac{4I^2L}{(1+6fL/\overline{v})^{1.67}} \tag{8}$$

where $S_v(f)$ denotes wind speed power spectral density, f is wind frequency in Hz, I denotes the turbulence intensity. Also, L is an integral scale parameter such that, $L = 20z$ for $z < 30\,m$ and $L = 600\,m$ for $> 30\,m$, where z is the height from sea level. In Eq. (8) $\overline{v}$ is the mean wind velocity, which can be computed using the logarithmic wind profile as

$$\overline{v}(z) = \frac{\overline{V}log(z/z_0)}{log(H/z_0)} \tag{9}$$

where $\overline{V}$ is the mean wind speed at the turbine reference height H at which the speed $\overline{V}$ is known, and z_0 is the roughness length of the ocean surface. In this study, mean wind speed is considered as $12\,m/s$, roughness of sea surface is $10^{-4}\,m$, and turbulence intensity is 10%.

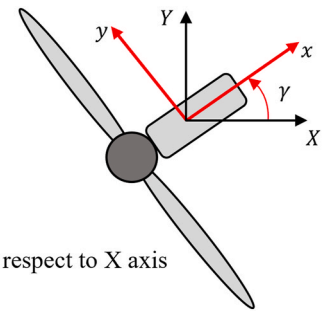

x: fore-aft direction

y: side-to-side direction

γ: yaw angle of wind turbine with respect to X axis

Fig. 4. Local and global coordinate systems of the OWT.

Wind loads are computed and represented in the local coordinate system (side-to-side as local y direction and fore-aft as local x direction) of the turbine as shown in Fig. 4. The simulated wind loads in OpenFAST are applied on the FE model along the fore-aft and side-side directions in this study. For FE model updating, the loads are projected to a global coordinate system, i.e., X-Y-Z in Fig. 4, where Z denotes upright direction. The wind loads at the local coordinate system are projected to the global coordinate system as

$$\mathbf{F}_{X-Y-Z} = \mathbf{T}\mathbf{F}_{x-y-z}, \mathbf{M}_{X-Y-Z} = \mathbf{T}\mathbf{M}_{x-y-z} \tag{10}$$

where the transformation matrix is

$$\mathbf{T} = \begin{bmatrix} \cos\gamma & -\sin\gamma & 0 \\ \sin\gamma & \cos\gamma & 0 \\ 0 & 0 & 1 \end{bmatrix} \tag{11}$$

In Eq. (10), the terms $\mathbf{F}_{X-Y-Z} = \begin{bmatrix} F_X^{Wind} & F_Y^{Wind} & F_Z^{Wind} \end{bmatrix}^T$ and $\mathbf{M}_{X-Y-Z} = \begin{bmatrix} M_X^{Wind} & M_Y^{Wind} & M_Z^{Wind} \end{bmatrix}^T$ are wind force and moment vectors in the global coordinate system, respectively, and $\mathbf{F}_{x-y-z} = \begin{bmatrix} F_x^{Wind} & F_y^{Wind} & F_z^{Wind} \end{bmatrix}^T$ and $\mathbf{M}_{x-y-z} = \begin{bmatrix} M_x^{Wind} & M_y^{Wind} & M_z^{Wind} \end{bmatrix}^T$ are wind force and moment vectors in the local coordinate system, respectively.

2.3.2. Wave load

As can be seen in Fig. 2, the jacket substructure is made of four cylindrical legs, and wave load is distributed over each leg. Morison's equation can be used to calculate the wave load acting on a slender cylindrical structure (Faltinsen, 1993), see Fig. 5. The wave load dF acting on a strip of length dz of the substructure can be expressed as

$$dF = \frac{1}{2}\rho D C_d |\dot{u}|\dot{u}dz + \frac{1}{4}\pi C_m D^2 \rho \ddot{u} dz \tag{12}$$

where $\rho = 1025\ kg/m^3$ is the density of the water, $D = 1.6\ m$ is the diameter of the substructure, and $C_d = 1.2$ and $C_m = 2$ represent the drag and mass coefficients, respectively. Moreover, the acceleration and velocity of water wave particles ($\ddot{u}$ and $\dot{u}$) can be determined using JONSWAP spectrum (IEC 61400-3-1:2019) as follows

$$S(f) = \frac{5}{16} H_s^2 T_\omega \left(\frac{f}{f_\omega}\right)^{-4} \alpha(1 - 0.287\ ln\,\gamma)\gamma^\beta \tag{13}$$

where f is frequency of the spectrum, $T_\omega = 10\ s$ is the wave period, $f_\omega = 1/T_\omega$ is the wave frequency, $H_s = 3m$ is the significant wave height, γ denotes the peakedness parameter (IEC 61400-3-1:2019), $\alpha = exp\left(-1.25(f/f_\omega)^{-4}\right)$, and $\beta = \exp\left(-\frac{(f-f_\omega)^2}{2\sigma^2 f_\omega^2}\right)$, where parameter σ can be computed as

$$\sigma = \begin{cases} 0.07 & f < f_\omega \\ 0.09 & f > f_\omega \end{cases} \tag{14}$$

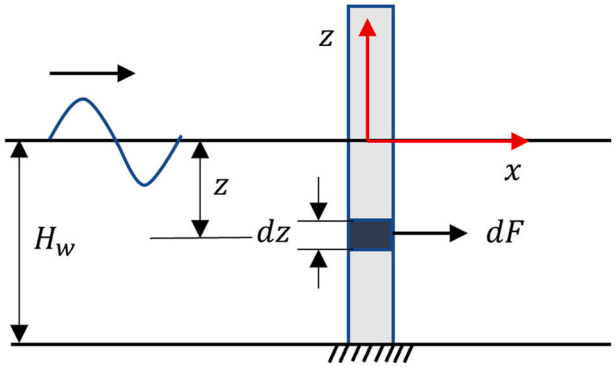

Fig. 5. Cylindrical substructure with wave load.

According to the JONSWAP spectrum, water particles velocity and acceleration can be determined as

$$\begin{aligned} \dot{u} &= \sum_{j=1}^{N} \omega_j A_j \frac{\cos h[k(z+H_w)]}{T_\omega \sin h(kH_w)} \sin(\omega_j t - k_j x + \phi_j) \\ \ddot{u} &= \sum_{j=1}^{N} \omega_j^2 A_j \frac{\cos h[k(z+H_w)]}{T_\omega \sin h(kH_w)} \cos(\omega_j t - k_j x + \phi_j) \end{aligned} \tag{15}$$

where ω is the wave frequency in rad/s, k is the wave number in $1/m$ and can be related to wave frequency ω and water depth z by the dispersion equation, $k\tanh(kz) = \omega^2/g$ where $g = 9.8\ m/s^2$, ϕ_j represents the uniform random phase angle distributed over $[0, 2\pi]$, $H_w = 27.75\ m$ is the water depth, and $A_j = \sqrt{2S(\omega_j)\Delta\omega}$ where $\Delta\omega = \omega_c/N$ in which ω_c represents the upper cut-off frequency and N denotes the number of frequency data points.

3. Case studies

In this section, the effect of sensor type, the number of sensors, and modeling errors on the accuracy of input loads and model parameter estimation are investigated through three case studies described in Table 3. In Case 1, assume that only wind forces as input and RNA mass as model parameters are unknown. In this case, the FE model used for simulation is the same as the model used for input/parameter estimation. Objective here is to investigate the effect of sensor type on input/parameter estimation, and to this end, only wind forces are considered. In Case 2, wind-induced moments are also included in the models to increase the number of unknown input loads, and the goal is to investigate the number of sensors on input/parameter estimation. Case 3 is considered to investigate the effect of input load assumptions and parameter errors on input/parameter estimation, so it is divided into two subcases (Case 3-1 and Case 3-2). In Case 3-1, the module of elasticity in the simulation model is different from the estimation model. In Case 3-2, wave load is included in the simulation model while neglected in the estimation model to understand the potential effects of various modeling errors on the model updating process in offshore wind turbine applications.

In the simulation model, the wind and wave loads generated from

Table 3
Summary of case studies.

Case name	Objective	Loads in the simulation model	Unknown Loads in the estimation model	Remarks
1	Investigating the effect of sensor type on input/parameter estimation	Wind forces only	Wind forces only	No modeling error
2	Investigating the effect of number of sensors on input/parameter estimation	Wind forces and moments	Wind forces and moments	No modeling error
3–1	Investigating the effect of model parameter error on input/parameter estimation	Wind forces and moments	Wind forces and moments	Model of elasticity in the simulation model is different with the estimation model
3–2	Investigating the effect of model input load error on input/parameter estimation	Wind and wave forces, and wind moments	Wind forces and moments	Inputs in the simulation model is different with the estimation model

OpenFAST and Morrison's equation, respectively, are applied to the FE model of the wind turbine. Then, responses of the structure are recorded and artificially polluted with Gaussian white noise, where noise to signal ratio is 1% for each measurement channel, i.e., RMS(noise) $= 0.01 \times$ RMS(measurement). The noisy responses are considered as synthetic measurement data. In the estimation model, wind loads and model parameters are unknown. The synthetic measurement data are integrated into the FEM model of the tower using the Bayesian inference method to estimate unknown wind loads and model parameters.

Fig. 6 (a) illustrates the top view of the tower, the local and global coordinate systems, and the wind and wave directions. Fig. 6 (b) shows the cross section of the tower top and the wind loads, and Fig. 6 (c) illustrates the cross section of the deck leg base and the wave loads. Fig. 7 shows the synthetic wind loads and their frequency spectra applied to the tower top in the local coordinate system. Fig. 8 displays the synthetic wave loads and their frequency spectra at deck leg base, which is located at sea level as shown in Figs. 3 and 6 (a) with a green color node. The wave loads are distributed over the substructure, and nodal forces and moments are accordingly calculated and applied to the FE model. The wave loads shown here are only in one direction, and they are assumed to be zero in other directions. The wind and wave loads are assumed to be in the same direction. While the interaction of wind and blades creates loads with different components in x and y directions, and the interaction of wave and substructure only creates a distributed force in one direction.

Synthetic measurement data include acceleration and strain responses at different locations along the tower as shown in Fig. 9. The green nodes represent accelerometers placed at heights of 26 *m*, 52 *m*, and top of the tower. The accelerometers are assumed to be biaxial, measuring acceleration responses in X and Y directions. The red nodes indicate the strain gauges placed at the base and middle height of the tower. There are four strain gauges at each section in order to estimate wind loads in X and Y directions. Each strain gauge can record axial strain only in the Z direction.

In system identification and model updating applications, identifiability or observability analysis can be utilized to decide about the most identifiable parameter sets, especially when dealing with large number of unknown parameters. However, most of the assessment frameworks are either for model parameters (Ebrahimian et al., 2019; Shi et al., 2021) or input loads (Martinelli, 2019), and a joint input-parameter identifiability assessment framework has not been developed for generic models (Maes et al., 2019). For a model parameter to be identifiable, the model response at measurement locations should be sensitive enough to the parameter, and the parameter should not have correlation or dependence on other unknown parameters. Adjusting the measurement locations, i.e., optimal sensor placement (Ercan et al., 2023; Ercan and Papadimitriou, 2023), can help with the identifiability problem. Regardless of the number of unknown parameters, as long as the unknown parameters remain identifiable, they can be estimated through the model updating process. In the current problem, for the given sensor array shown in Fig. 9, it was found that only RNA mass and wind loads applied to the tower top can be jointly estimated accurately.

Characterizing the aerodynamic damping in wind turbine modeling can often be challenging (Hansen, 2015; Hansen et al., 2006; Stäblein et al., 2017). Aerodynamic damping stems from the wind-blade interaction and it can affect the blade dynamics, which is transferred to the tower top as force components. In this study, the estimated input wind loads embody both the interactions of wind-blades and tower-blades; thus, they will include the effects of aerodynamic damping.

To implement the window-based Bayesian inference approach for joint input loads and model parameter estimation, window parameters, and filter hyperparameters should be selected carefully. Tunning the hyperparameter was investigated in previous studies (Ebrahimian et al., 2015, 2018). Here the effects of different hyperparameters are discussed briefly.

- The window length and sliding stride are set to 100- and 80-time steps, respectively. It was founded in Ebrahimian et al. (2018) that large window length improves the input load estimation accuracy but increases the computational cost. On the other hand, small window length does not embody enough system responses, i.e., the short window is not informative enough to estimate the input loads accurately. There is a trade-off between estimation accuracy and computational cost to select proper window length.
- The initial value of the model parameters and associated covariance matrix at the first window is set as $\widehat{\boldsymbol{\theta}}_0 = 0.8\widehat{\boldsymbol{\theta}}_{true}$ and $(\widehat{\boldsymbol{P}}_{\boldsymbol{\theta}})_0 = diag(p_\theta \widehat{\boldsymbol{\theta}}_0)^2$, where $\widehat{\boldsymbol{\theta}}_{true}$ is the true value of the model parameter (RNA mass), and $p_{\boldsymbol{\theta}} = 0.3$ is the coefficient of variation (CoV) of the initial parameter estimate. Generally, the covariance matrix $(\widehat{\boldsymbol{P}}_{\boldsymbol{\theta}})_0$ quantifies the uncertainties in the initial parameter estimate. It is a diagonal matrix, which indicates the parameters are statistically uncorrelated. Increasing CoV, $p_{\boldsymbol{\theta}}$, introduces more uncertainty to the initial value of the model parameters. In this condition, the Bayesian filtering process relies more on the discrepancies between the predicted and measured responses than the initial values to update the parameters. Higher value of $p_{\boldsymbol{\theta}}$ may accelerate the parameter estimation process but may also destabilize the estimation process (Ebrahimian et al., 2015; Hoshiya and Saito, 1984; Simon, 2006).
- The initial values of load estimate $\widehat{\mathbf{u}}^T_{t_1^1:t_2^1,0}$ at the first window is zero, and the covariance matrix of load estimate is a diagonal matrix with diagonal entries $(s_{\mathbf{u}} p_{\mathbf{u}})^2$, where $s_u = 1000$ denotes a scaling factor indicating the order of magnitude of the wind loads, and p_u is the initial standard deviation of the wind loads which are set as $p_{\mathbf{u}} = 0.5$ kN for input forces and $p_u = 0.5$ kN.m for input moments. By setting the value of $p_{\boldsymbol{u}}$, we can regularize the estimation process or enforce

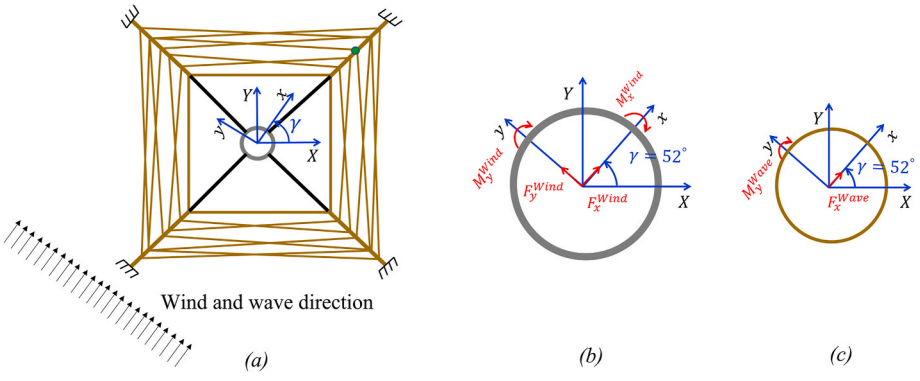

Fig. 6. (a) Top view of the wind turbine and coordinate systems, (b) cross section of the tower top and direction of wind loads, and (c) cross section of the deck leg base and direction of wave loads.

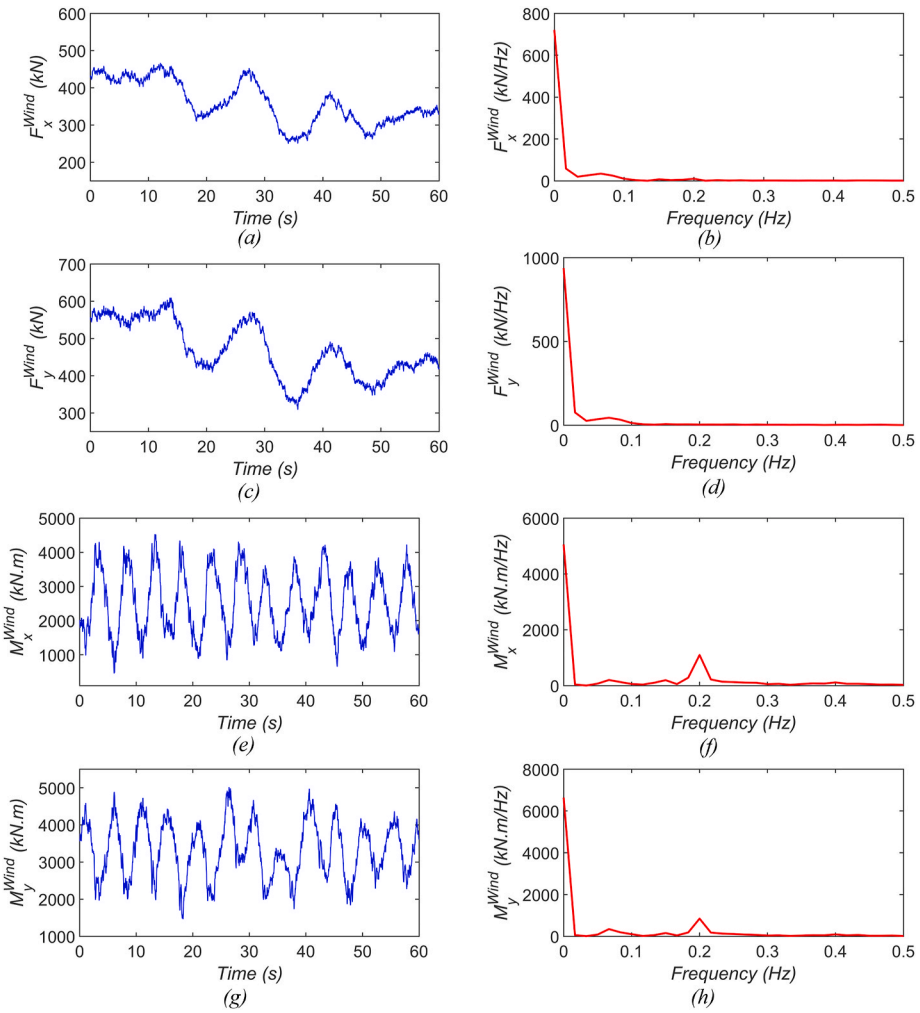

Fig. 7. Synthetic wind loads applied to the tower top, (a,b) wind force time history and its frequency spectrum in the x direction, (c,d) wind force time history and its frequency spectrum in the y direction, (e,f) wind moment time history and its frequency spectrum in the x direction, and (g,h) wind moment time history and its frequency spectrum in the y direction.

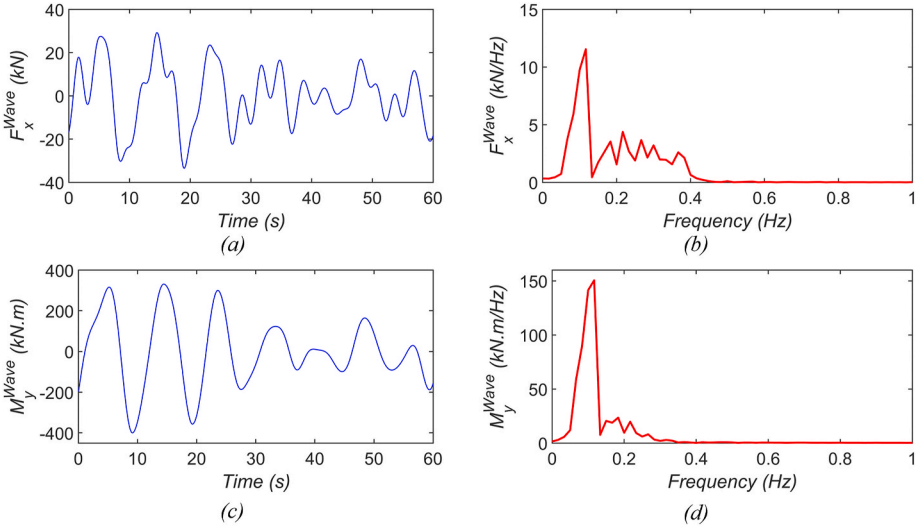

Fig. 8. Synthetic wave loads at deck leg base, (a,b) wave force time history and its frequency spectrum in the x direction, (c,d) wave moment time history and its frequency spectrum in the x direction.

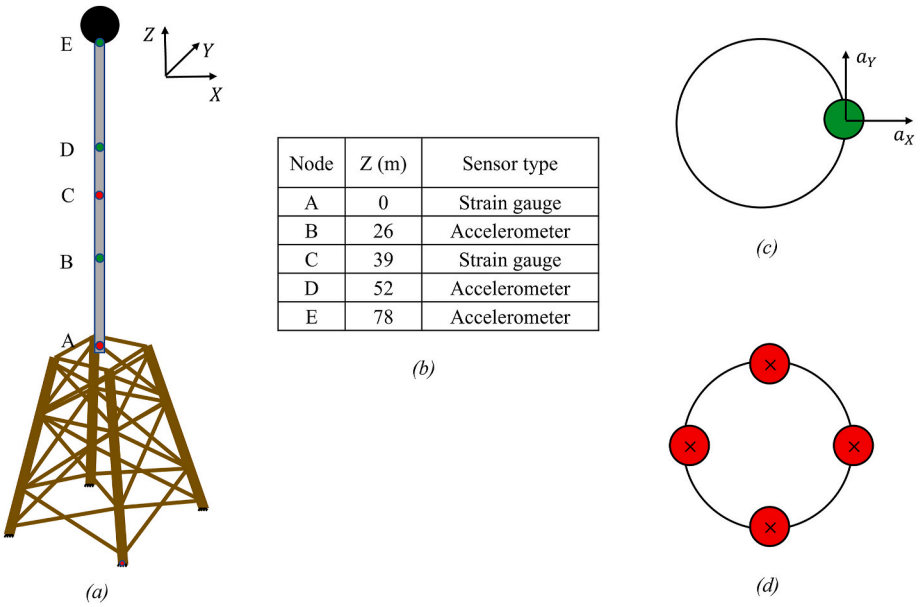

Node	Z (m)	Sensor type
A	0	Strain gauge
B	26	Accelerometer
C	39	Strain gauge
D	52	Accelerometer
E	78	Accelerometer

Fig. 9. (a) Sensor array on the tower, (b) sensor locations measured from the tower base, (c) biaxial accelerometers, and (d) uniaxial strain gauges.

smoothness on the loads estimate (Aster et al., 2018; Dashti and Stuart, 2017; Mohammad-Djafari, 2021). The small value of $p_{\mathbf{u}}$ results in smoother input load estimates, and the algorithm trusts more on prior information; however, the large value of $p_{\mathbf{u}}$ makes the algorithm sensitive to the measurement data, and the estimated loads can become noisy (Ebrahimian et al., 2018).

- The covariance matrix of the perturbation term in Eq. (6) is expressed as a diagonal matrix with two diagonal submatrices $\mathbf{Q}_{\boldsymbol{\theta}}$ and $\boldsymbol{Q}_{u}$, where the matrix $\mathbf{Q}_{\boldsymbol{\theta}}$ associated with parameter perturbation is set as $\mathbf{Q}_{\boldsymbol{\theta}} = diag(q_{\boldsymbol{\theta}}\widehat{\boldsymbol{\theta}}_0)^2$ with the coefficient of variation $q_{\boldsymbol{\theta}} = 10^{-3}$, and the matrix $\mathbf{Q}_{\mathbf{u}}$ associated with load perturbation is a diagonal matrix with entries $(q_{\mathbf{u}})^2$ and the standard deviation value is set to $q_{\mathbf{u}} = 10^{-2}$. The perturbation term adds perturbation to the iterative process, whereby the large value of the perturbation variance improves the convergence speed but might cause instability of the algorithm; conversely, the smaller value of perturbation variance deaccelerates the convergence of the process (Ebrahimian et al., 2018).
- Moreover, the covariance matrix of measurement error $\mathbf{R}$ is a diagonal matrix with entries $\left(r_f \times RMS(\mathbf{y})\right)^2$, where $r_f = 10^{-2}$ is noise-to-signal ratio (NSR), and $RMS(\mathbf{y})$ denotes root mean square of the measurement data. The value of NSR depends on the quality of measurement data. The higher NSR enforces the algorithm to rely more on the prior information about the parameters than the measurements. It will also slow down the convergence process. However, small values indicate trustworthy data, and the estimation process becomes sensitive to the discrepancies between the predicted and measured responses, which may destabilize the estimation process. Generally, the statistics of measurement error are unknown but can be estimated based on the sensor properties. Moreover, adaptive Bayesian filtering can be employed to estimate measurement error covariance matrix based on measurement data (Akhlaghi et al., 2018; Nabiyan et al., 2023).

The estimation process follows the steps described in Table 1. OpenSees is used to predict the response of the structure in the local coordinate system given model parameters and input loads, then it interfaces with MATLAB to use the responses for model updating. The predicted responses are transformed to the global coordinate system in MATLAB, the model parameters are updated, and wind loads are estimated in the global coordinate system. Afterward, the estimated parameter and wind loads are shared with OpenSees in the local coordinate system for the next iteration. In the following case studies, results are shown in the global coordinate system, which is independent of turbine orientation or yaw angle.

3.1. Case 1: investigating the effect of sensor types on input load and model parameter estimation

In this case, the effect of sensor types such as strain gauge and accelerometer on input wind loads and parameter estimation is investigated. In this simplest case study, only wind forces are considered as the source of excitation or input. The tower structure response is simulated by applying wind forces in X and Y directions in the global coordinate system. Three sets of measurement are considered in this case as listed in Table 4. In the model updating process, it is assumed that wind forces in the X and Y directions and RNA mass are unknown and to be estimated by employing the Bayesian inference framework.

Fig. 10 shows time history and frequency spectrum of the nominal/true forces and those estimated according to the data of three sensor sets. As can been observed, the estimated forces based on Set 1, including only accelerations, show low-frequency drifts. These drifts appear because the dynamic response is not sensitive to low-frequency component of the input forces, i.e., quasi-static forces (Eftekhar Azam et al., 2015; Lourens et al., 2012; Valikhani and Younesian, 2019). Conversely, the estimated forces based on Set 2, including only strain data have high-frequency oscillations. This effect is due to the reason that strain data are not sensitive to high frequency forces. However, the combination of acceleration and strain measurements provide the most accurate estimation of input forces in a broader frequency range as shown in Fig. 10 (a)–(d). Fig. 11 shows the convergence history of the estimated RNA mass (normalized by true value of RNA mass which is not

Table 4
Sensor types and their placement on the tower for Case 1.

Set Name	Sensor types and their placement
Set **1**	3 accelerometers located at nodes B, D, and E as shown in Fig. 9
Set **2**	4 strain gauges at node A as shown in Fig. 9
Set **3**	3 accelerometers at nodes B, D, and E and 4 strain gauges at node A as shown in Fig. 9

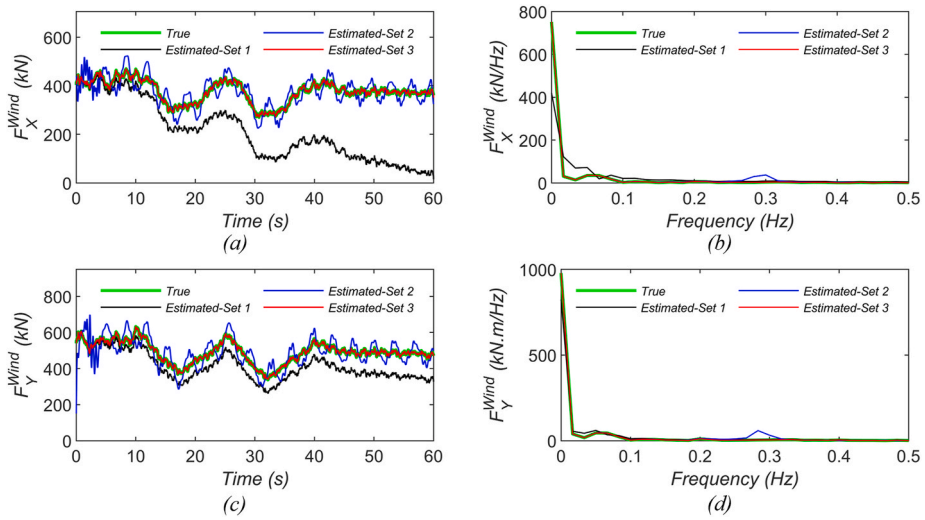

Fig. 10. Time history and frequency spectrum of true and estimated wind forces for different sensor sets, (a,b) X direction, (c,d) Y direction for Case 1.

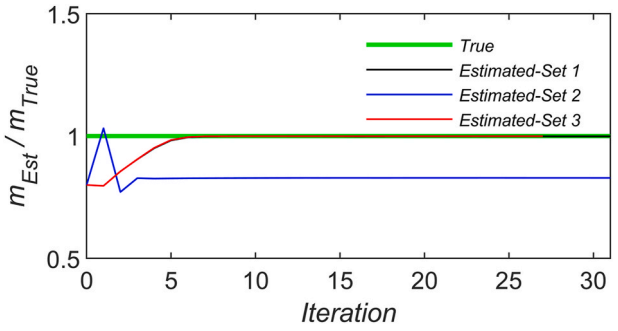

Fig. 11. Convergence history of normalized RNA mass for different sensor sets for Case 1.

disclosed due to confidentiality) using different sensor sets. The nacelle mass can be estimated accurately if the dataset includes acceleration measurements, as in Set 1 and Set 3. Strain data do not include the mid- and high-frequency responses to which the RNA mass contributes, so Set 2 is not informative to estimate RNA mass.

3.2. Case 2: investigating the effect of the number of sensors on input load and model parameter estimation

In this case, the effect of the number of sensors on wind load and model parameter estimation is studied. To this end, the dynamic response is simulated from the FE model of the tower by applying the wind loads, including wind forces and moments in X and Y directions. Two sensor sets are considered to record synthetic data as tabulated in Table 5. In the model updating process, it is assumed that wind loads, i.e., forces and moments at the tower top in X and Y directions are unknown to be estimated.

Fig. 12 compares the estimated forces and moments in X and Y directions at time and frequency domains based on the two sensor sets. As can be seen, the estimated loads based on both sets have high-amplitude oscillations at the beginning of the time history, which is because of the effect of non-zero initial conditions. In the beginning of the estimation window, we assumed at-rest initial condition. This is done to replicate a real-world monitoring condition. Moreover, the estimated loads based on the Set 1 display low-frequency drifts. These drifts are because of the insufficient number of strain gauge sensors. When data are recorded in one section of the tower, force and moments cannot be estimated uniquely, so additional strain data in Set 2 improves the load estimation accuracy.

Fig. 13 shows the convergence history of normalized estimated RNA mass for the two sensor sets. As can been seen, RNA mass can be estimated accurately for both sets. Each set contains acceleration data, which are sufficient to estimate the RNA mass.

Table 5
Sensor types and their placement on the tower for Case2.

Set Name	Sensor types and their placement
Set **1**	3 accelerometers at nodes B, D, and E and 4 strain gauges at node A as shown in Fig. 9
Set **2**	3 accelerometers at nodes B, D, and E and 8 strain gauges at nodes A and C as shown in Fig. 9

3.3. Case 3: investigating the effect of modeling errors on input load and model parameter estimation

In this Section, two different sources of modeling errors are investigated. In Case 3-1, the effect of model parameter error is investigated, and in Case 3-2, the effect of input load error is investigated.

Case 3-1. The effect of model parameter error

The modulus of elasticity is an important stiffness-related parameter in the FE modeling of an OWT structure. While the variation of this parameter is not significant for steel material in practice, deviation from the nominal values is possible due to, for example, manufacturing defects, corrosion, or other sources of operational deterioration. In previous case studies, the modulus of elasticity was considered similar between the simulation and estimation models. This case study investigates the effect of error in the modulus of elasticity on wind load and RNA mass estimation. To this end, synthetic data are generated using the FE model of the tower with the modulus of elasticity $E = 190$ GPa. In the model updating process, the modulus of elasticity in the FE model is assumed to be $E = 200$ GPa, i.e., 5% error is introduced to the modulus of elasticity. Input loads in the simulation and parameter estimation models are similar, i.e., they include wind forces and moments in the X and Y directions. Sensor types and locations are the same as Set 2 described in Table 5.

Fig. 14 shows the time history and frequency spectrum of true and estimated loads for this case study. The estimated loads in X and Y directions include low-frequency drifts, which appear as a baseline and are due to the error in the modulus of elasticity. The wind loads have significant energy at the low-frequency band, and the response of the

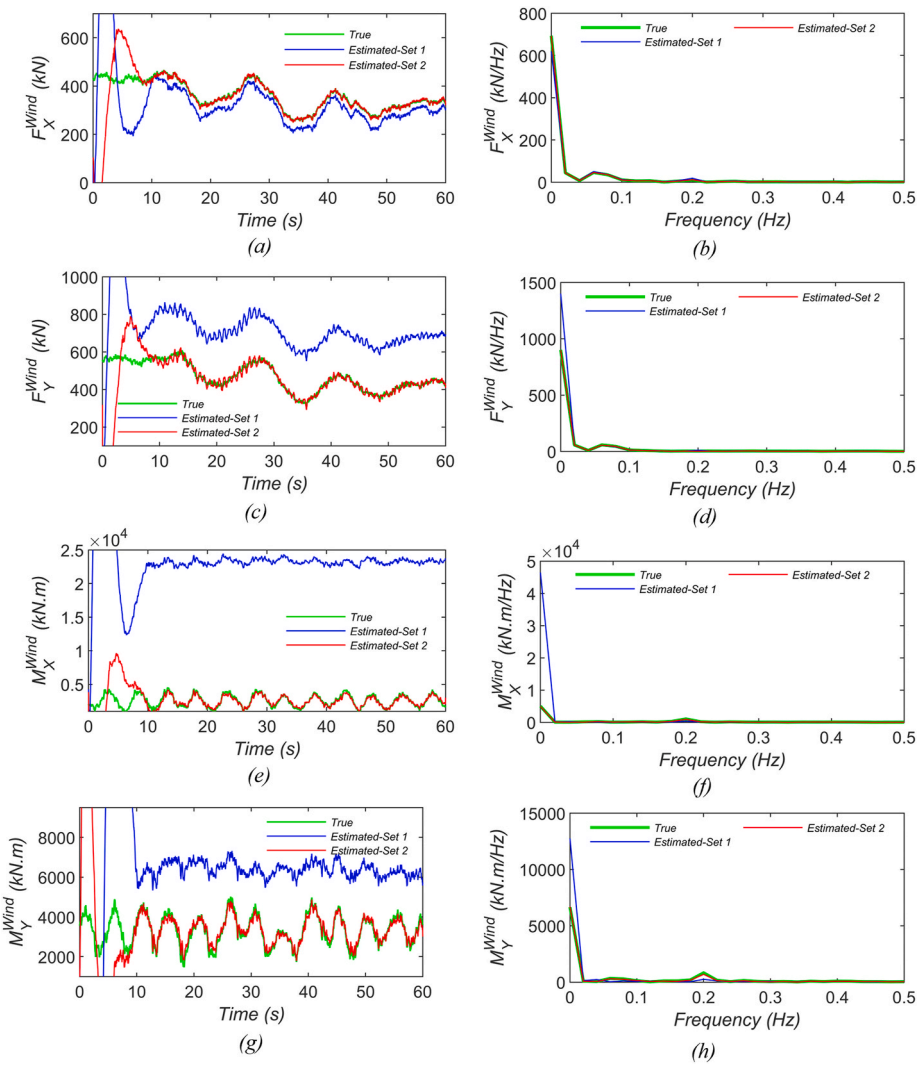

Fig. 12. Time history and frequency spectrum of true and estimated wind loads for two sensor sets, (a,b) forces in the X direction, (c,d) forces in the Y direction, (e,f) moments in the X direction, and (g,h) moments in the Y direction for Case 2.

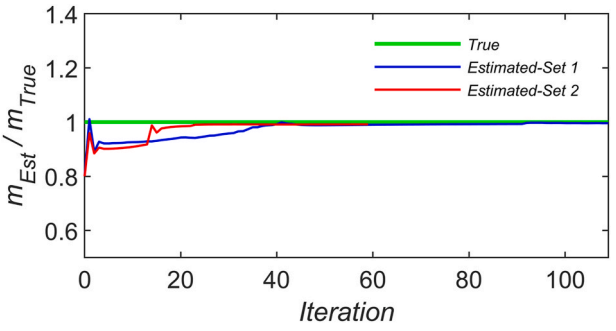

Fig. 13. Convergence history of normalized RNA mass according to the data of two sensor sets for Case 2.

structure subjected to low-frequency loads is mostly controlled by the stiffness properties of the model. Therefore, the error in the modulus of elasticity is compensated for by a drift in the estimated wind loads. Fig. 15 displays the convergence history of the normalized RNA mass. As can been seen, the estimated RNA mass is higher than the true value, which is the result of the modeling error in the modulus of elasticity.

Case 3-2. The effect of input load error

The dynamic response of an OWT structure to wave loads is often insignificant compared to wind loads, due to the amplitude and application location of wave loads. Nevertheless, wave loads will be a source of modeling error if not accounted for correctly in the model updating process. The objective of this case study is to investigate the potential impacts of neglecting wave loads in the joint wind load and model parameter estimation. For this purpose, both wind and wave loads are considered in the simulation model, but only wind loads are considered and estimated in the model updating process. Sensor type and array are the same as Set 2 as described in Table 5.

Fig. 16 shows the time history and frequency spectrum of true and estimated wind loads for the case where the effects of wave loads are neglected in the model updating process. As can be observed, the estimated wind loads match the true loads. The reason is likely due to the high stiffness of the jacket substructure and the relatively low amplitude of wave loads, which cannot excite the system considerably. Fig. 17 displays the convergence history of the estimated RNA mass for the case having error in input loads. As can be seen, the error in the input loads has little impact on the RNA mass estimation.

4. Conclusions

Estimation of input loads and mechanics-based model parameters characterizing the dynamic response of offshore wind turbine (OWT)

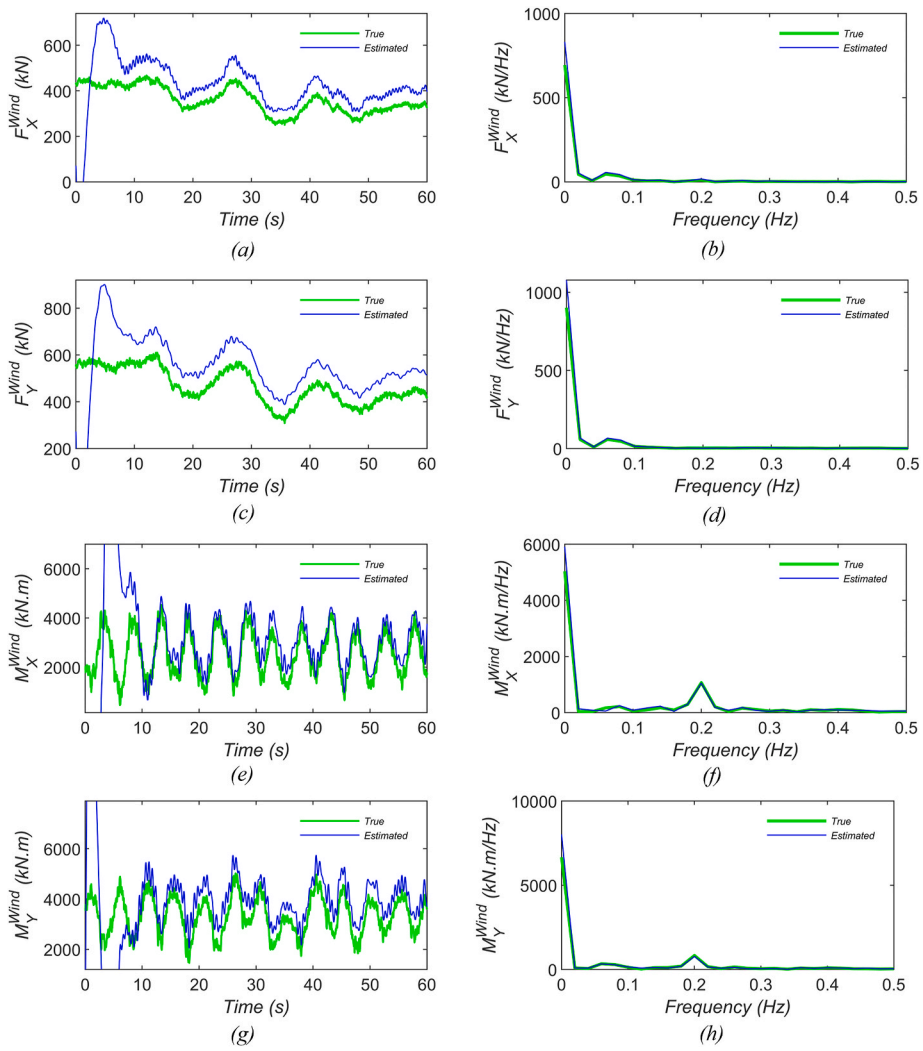

Fig. 14. Time history and frequency spectrum of true and estimated wind loads based on the model with error in modulus of elasticity, (a,b) forces in the X direction, (c,d) forces in the Y direction, (e,f) moments in the X direction, and (g,h) moments in the Y direction for Case 3-1.

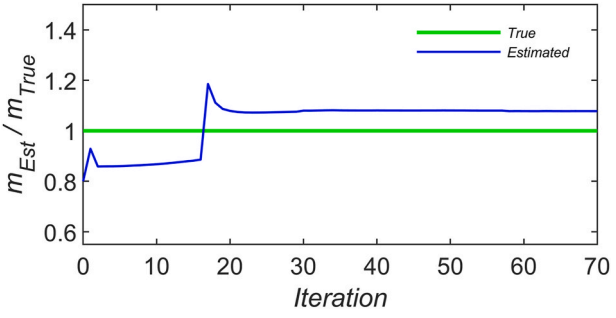

Fig. 15. Convergence history of normalized RNA mass based on the model with error in modulus of elasticity for Case 3-1.

structures is important for health monitoring, digital twinning, and remaining useful life prediction of these assets. In this study, a time-domain Bayesian inference method was presented to estimate input wind loads and rotor-nacelle assembly (RNA) mass in an OWT based on the dynamic response of the tower. The objective was to investigate the potential and limitations of the presented inference approach. Three fundamental questions pertaining to wind load and model parameter estimation were investigated through three different case studies using synthetically simulated data. These cases include the effects of sensor type (Case 1), number of sensors (Case 2), and modeling error (Case 3) on the estimation results. The first case study showed that the combination of acceleration and strain measurements are essential for accurate estimation of wind loads and RNA mass. Acceleration response is sensitive to high-frequency loadings while strain response is sensitive to low-frequency loading. Their combination yields the best wind load estimation capacity in broad frequency band. The second case study demonstrated that sensors should be deployed at different levels of the tower to enable the estimation of all components of wind loading including forces and moments. In the studied case, acceleration and strain data at two cross-sections along the tower height were required for a unique estimation of the wind forces and moments. In the third case study, the effect of two modeling errors including model parameter error (inaccurate modulus of elasticity) and input load error (neglected wave loads) in the model updating process were investigated. For the model parameter error case, wind load estimates were affected by the modeling error, which caused a low-frequency drift in the estimated wind loads. In the case of model input load error, the studied case results showed that neglecting wave loads in the model updating process will likely have negligible effects on the wind load estimation. This is due to the low impact of the wave loads on the dynamic response of the OWT tower and the high stiffness of the substructure to which the wave loads were applied in the considered case study.

The framework proposed in this paper can be used for monitoring

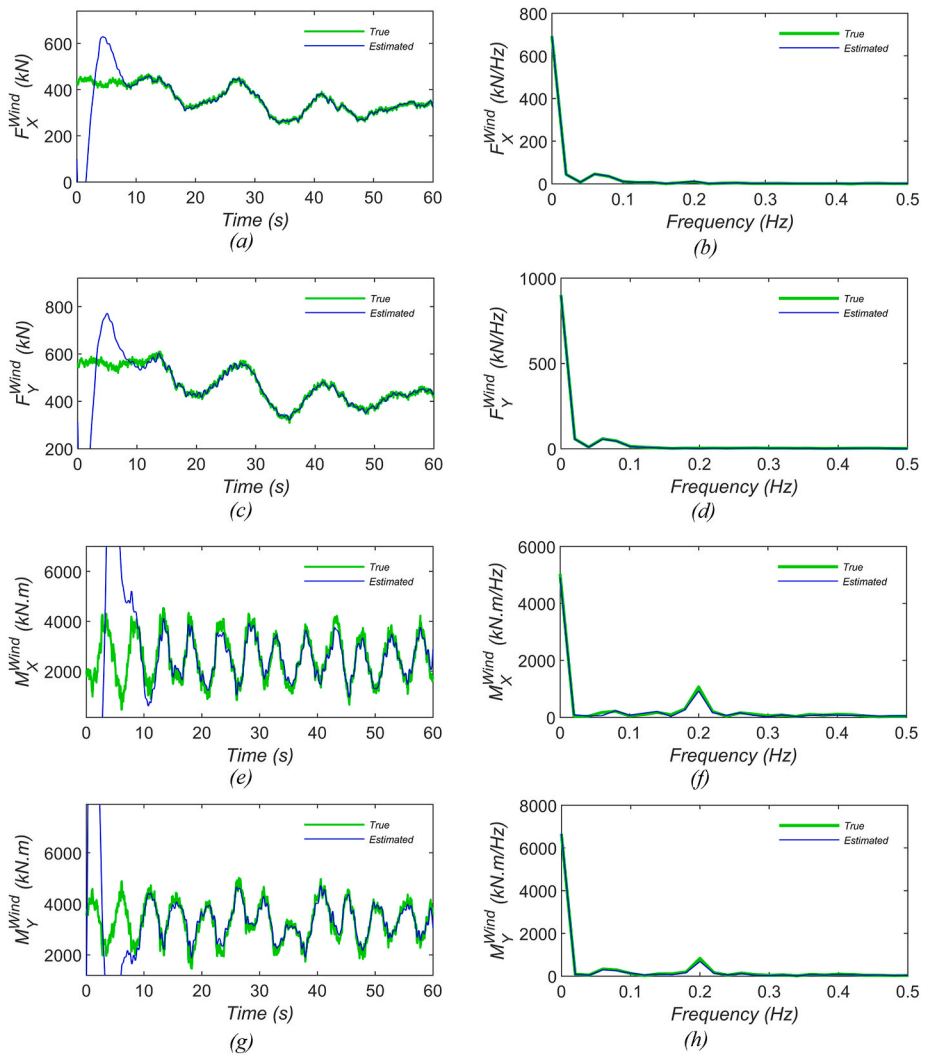

Fig. 16. Time history and frequency spectrum of true and estimated wind loads based on the model with error in input loads, (a,b) forces in the X direction, (c,d) forces in the Y direction, (e,f) moments in the X direction, and (g,h) moments in the Y direction for Case 3-2.

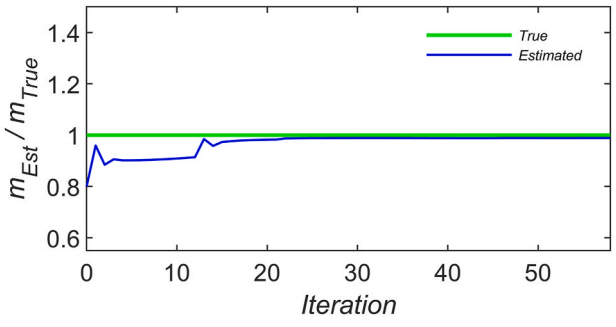

Fig. 17. Convergence history of normalized RNA mass based on the model with error in input loads for Case 3-2.

and estimating parameters including model parameters and loads that can affect the structural responses. The marine condition has a stochastic dynamic nature, and it can cause change in the properties of structures and loadings. For example, extreme events such as storms in the ocean can apply significant loads to OWT structures, or temperature variation might change the properties of composite materials in blades, so it might affect the blade-tower interaction forces. If the environmental and operational conditions can be represented by parameters, then the Bayesian framework can be used to estimate those parameters from the structural responses. The parameters are identifiable if the measured responses are informative enough about the parameters, and also the parameters should be uncorrelated or independent; otherwise, the environment conditions will result in modeling error.

This study highlighted the importance of instrumentation, including sensor type and number, and modeling error in input load and model parameter estimation in OWTs. The combination of different sensors provides informative data to accurately estimate model parameters and wind loads in broader frequency band without having low-frequency drifts or high-frequency oscillations. Moreover, accurate and unique joint input-parameter estimation is possible with adequate number of sensors installed at locations where the structural responses are sensitive to the estimation quantities. Modeling error is a challenging issue in the model updating process and can result in biased estimations, as seen in the case of model parameter error. Generally, the effect of modeling error can be reduced if sources of error can be identified, and error characteristics can be quantified. The study included two main limitations. First, it has been performed using synthetic data through idealized case studies. In real-world problems, the data include measurement noise with unknown statistics. Second, the study did not offer a holistic and comprehensive approach to find the optimal type, number, and placement of sensors for different estimation objectives. This can be the subject of future work. Nevertheless, the study illuminated important

physical facts about the application of time-domain Bayesian inference for joint input-parameter estimation in OWTs, which can guide future research efforts.

CRediT authorship contribution statement

Mohammad Valikhani: Writing – review & editing, Writing – original draft, Visualization, Software, Methodology, Investigation. **Mansureh Nabiyan:** Writing – review & editing, Software, Methodology, Investigation, Conceptualization. **Mingming Song:** Writing – review & editing, Software, Methodology. **Vahid Jahangiri:** Writing – review & editing, Writing – original draft, Methodology. **Hamed Ebrahimian:** Writing – review & editing, Supervision, Methodology, Conceptualization. **Babak Moaveni:** Writing – review & editing, Supervision, Conceptualization.

Declaration of competing interest

The authors declare that they have no known competing financial interests or personal relationships that could have appeared to influence the work reported in this paper.

Acknowledgments

The authors acknowledge the support of this study by the National Offshore Wind Research and Development Consortium (NOWRDC) under contract #154719, and the National Science Foundation Partnerships for International Research and Education (NSF PIRE) award #2230630.

References

Akhlaghi, S., Zhou, N., Huang, Z., 2018. Adaptive adjustment of noise covariance in Kalman filter for dynamic state estimation. In: IEEE Power and. Energy Society General Meeting. https://doi.org/10.1109/PESGM.2017.8273755.

Aster, R.C., Borchers, B., Thurber, C.H., 2018. Parameter Estimation and Inverse Problems. Parameter Estimation and Inverse Problems, pp. 1–404. https://doi.org/10.1016/C2015-0-02458-3.

Augustyn, D., Smolka, U., Tygesen, U.T., Ulriksen, M.D., Sørensen, J.D., 2020. Data-driven model updating of an offshore wind jacket substructure. Appl. Ocean Res. 104. https://doi.org/10.1016/J.APOR.2020.102366.

Bathe, K.-J., 2006. Finite Element Procedures. Klaus-Jurgen Bathe.

Chopra, A.K., 2007. Dynamics of Structures. Pearson Education India.

Dai, K., Wang, Y., Huang, Y., Zhu, W., Xu, Y., 2017. Development of a modified stochastic subspace identification method for rapid structural assessment of in-service utility-scale wind turbine towers. Wind Energy 20, 1687–1710. https://doi.org/10.1002/WE.2117.

Dashti, M., Stuart, A.M., 2017. The bayesian approach to inverse problems. Handbook of Uncertainty Quantification 311–428. https://doi.org/10.1007/978-3-319-12385-1_7/COVER.

Devriendt, C., Magalhães, F., Weijtjens, W., De Sitter, G., Lvaro, Cunha A., Guillaume, P., 2014. Structural health monitoring of offshore wind turbines using automated operational modal analysis. Struct. Health Monit. 13, 644–659. https://doi.org/10.1177/1475921714556568.

Ebrahimian, H., Astroza, R., Conte, J.P., 2015. Extended Kalman filter for material parameter estimation in nonlinear structural finite element models using direct differentiation method. Earthq. Eng. Struct. Dynam. 44, 1495–1522. https://doi.org/10.1002/EQE.2532.

Ebrahimian, H., Astroza, R., Conte, J.P., Bitmead, R.R., 2019. Information-theoretic approach for identifiability assessment of nonlinear structural finite-element models. J. Eng. Mech. 145, 4019039.

Ebrahimian, H., Astroza, R., Conte, J.P., Papadimitriou, C., 2018. Bayesian optimal estimation for output-only nonlinear system and damage identification of civil structures. Struct. Control Health Monit. 25, e2128. https://doi.org/10.1002/STC.2128.

Eftekhar Azam, S., Chatzi, E., Papadimitriou, C., 2015. A dual Kalman filter approach for state estimation via output-only acceleration measurements. Mech. Syst. Signal Process. 60, 866–886. https://doi.org/10.1016/J.YMSSP.2015.02.001.

Ercan, T., Papadimitriou, C., 2023. Bayesian optimal sensor placement for parameter estimation under modeling and input uncertainties. J. Sound Vib. 563. https://doi.org/10.1016/j.jsv.2023.117844.

Ercan, T., Sedehi, O., Katafygiotis, L.S., Papadimitriou, C., 2023. Information theoretic-based optimal sensor placement for virtual sensing using augmented Kalman filtering. Mech. Syst. Signal Process. 188. https://doi.org/10.1016/j.ymssp.2022.110031.

Fallais, D.J.M., Voormeeren, S., Lourens, E., 2016. Vibration-based identification of hydrodynamic loads and system parameters for offshore wind turbine support structures. Energy Proc. 94, 191–198. https://doi.org/10.1016/J.EGYPRO.2016.09.222.

Faltinsen, O., 1993. Sea Loads on Ships and Offshore Structures, vol. 340. Cambridge University Press. Cambridge University Press.

Flores Terrazas, V., Sedehi, O., Papadimitriou, C., Katafygiotis, L.S., 2022. A streamline approach to multiaxial fatigue monitoring using virtual sensing. Struct. Control Health Monit. 29. https://doi.org/10.1002/stc.2863.

Friswell, M.I., Mottershead, J.E., 1995. Finite Element Modelling. Springer.

Ghahari, F., Malekghaini, N., Ebrahimian, H., Taciroglu, E., 2022. Bridge digital twinning using an output-only bayesian model updating method and recorded seismic measurements. Sensors 22. https://doi.org/10.3390/s22031278.

Ghahari, S.F., Abazarsa, F., Ebrahimian, H., Taciroglu, E., 2020. Output-only model updating of adjacent buildings from sparse seismic response records and identification of their common excitation. Struct. Control Health Monit. 27, e2597. https://doi.org/10.1002/STC.2597.

Hansen, M., 2015. Aerodynamics of Wind Turbines. Routledge.

Hansen, M.H., Thomsen, K., Fuglsang, P., Knudsen, T., 2006. Two methods for estimating aeroelastic damping of operational wind turbine modes from experiments. In: Wind Energy. https://doi.org/10.1002/we.187.

Hines, E.M., Baxter, C.D.P., Ciochetto, D., Song, M., Sparrevik, P., Meland, H.J., Strout, J. M., Bradshaw, A., Hu, S.L., Basurto, J.R., Moaveni, B., 2023. Structural instrumentation and monitoring of the block Island offshore wind Farm. Renew. Energy 202, 1032–1045. https://doi.org/10.1016/J.RENENE.2022.11.115.

Hoshiya, M., Saito, E., 1984. Structural identification by extended Kalman filter. J. Eng. Mech. 110, 1757–1770.

Hu, J., Lam, H.F., Yang, J.H., 2018. Operational modal identification and finite element model updating of a coupled building following Bayesian approach. Struct. Control Health Monit. 25, e2089. https://doi.org/10.1002/STC.2089.

IEC 61400-3-1:2019 | IEC Webstore [WWW Document], n.d. URL https://webstore.iec.ch/publication/29360 (accessed 4.10.24).

Igwemezie, V., Mehmanparast, A., Kolios, A., 2019. Current trend in offshore wind energy sector and material requirements for fatigue resistance improvement in large wind turbine support structures–A review. Renew. Sustain. Energy Rev. 101, 181–196.

Jacobsen, N.-J., Andersen, P., Brincker, R., 2007. Eliminating the influence of harmonic components in operational modal analysis. In: Conference Proceedings : IMAC-XXIV : A Conference & Exposition on Structural Dynamics.

James III, G.H., Carne, T.G., Lauffer, J.P., 1993. The Natural Excitation Technique (NExT) for Modal Parameter Extraction from Operating Wind Turbines.

Jonkman, B.J., Buhl, M.L., 2005. TurbSim User's Guide.

Lourens, E., Papadimitriou, C., Gillijns, S., Reynders, E., de Roeck, G., Lombaert, G., 2012. Joint input-response estimation for structural systems based on reduced-order models and vibration data from a limited number of sensors. Mech. Syst. Signal Process. 29, 310–327. https://doi.org/10.1016/J.YMSSP.2012.01.011.

Maes, K., Chatzis, M.N., Lombaert, G., 2019. Observability of nonlinear systems with unmeasured inputs. Mech. Syst. Signal Process. 130, 378–394.

Maes, K., Iliopoulos, A., Weijtjens, W., Devriendt, C., Lombaert, G., 2016. Dynamic strain estimation for fatigue assessment of an offshore monopile wind turbine using filtering and modal expansion algorithms. Mech. Syst. Signal Process. 76–77, 592–611. https://doi.org/10.1016/J.YMSSP.2016.01.004.

Maes, K., Weijtjens, W., de Ridder, E.J., Lombaert, G., 2018. Inverse estimation of breaking wave loads on monopile wind turbines. Ocean Eng. 163. https://doi.org/10.1016/j.oceaneng.2018.05.049.

Martinelli, A., 2019. Nonlinear unknown input observability: extension of the observability rank condition. IEEE Trans. Automat. Control 64. https://doi.org/10.1109/TAC.2018.2798806.

MathWorks Inc., 2022. MATLAB Version: 9.13.0 (R2022b).

McKenna, F., Fenves, G.L., Scott, M.H., others, 2000. Open System for Earthquake Engineering Simulation. University of California, Berkeley, CA.

Mehrjoo, A., Song, M., Moaveni, B., Papadimitriou, C., Hines, E., 2022. Optimal sensor placement for parameter estimation and virtual sensing of strains on an offshore wind turbine considering sensor installation cost. Mech. Syst. Signal Process. 169. https://doi.org/10.1016/j.ymssp.2021.108787.

Mohammad-Djafari, A., 2021. Regularization, bayesian inference, and machine learning methods for inverse problems. Entropy 23. https://doi.org/10.3390/E23121673.

Moriarty, P.J., Hansen, A.C., 2005. AeroDyn theory manual. https://doi.org/10.2172/15014831.

Moynihan, B., Mehrjoo, A., Moaveni, B., McAdam, R., Rüdinger, F., Hines, E., 2023. System identification and finite element model updating of a 6 MW offshore wind turbine using vibrational response measurements. Renew. Energy 219, 119430.

Nabiyan, M.S., Khoshnoudian, F., Moaveni, B., Ebrahimian, H., 2021. Mechanics-based model updating for identification and virtual sensing of an offshore wind turbine using sparse measurements. Struct. Control Health Monit. 28, e2647. https://doi.org/10.1002/STC.2647.

Nabiyan, M.-S., Sharifi, M., Ebrahimian, H., Moaveni, B., 2023. A variational Bayesian inference technique for model updating of structural systems with unknown noise statistics. Front Built Environ 9, 1143597.

Naets, F., Croes, J., Desmet, W., 2015. An online coupled state/input/parameter estimation approach for structural dynamics. Comput. Methods Appl. Mech. Eng. 283, 1167–1188. https://doi.org/10.1016/J.CMA.2014.08.010.

Noppe, N., Tatsis, K., Chatzi, E., Devriendt, C., Weijtjens, W., 2018. Fatigue stress estimation of offshore wind turbine using a Kalman filter in combination with accelerometers. In: Proceedings of ISMA 2018 - International Conference on Noise

and Vibration Engineering and USD 2018 - International Conference on Uncertainty in Structural Dynamics.
NREL, 2022. OpenFAST Documentation, V3.0.0.
Oliveira, G., Magalhaes, F., Cunha, Á., Caetano, E., 2016. Development and implementation of a continuous dynamic monitoring system in a wind turbine. J Civ Struct Health Monit 6, 343–353.
Ozbek, M., Rixen, D.J., 2013. Operational modal analysis of a 2.5 MW wind turbine using optical measurement techniques and strain gauges. Wind Energy 16, 367–381. https://doi.org/10.1002/WE.1493.
Peeters, B., de Roeck, G., 1999. Reference-based stochastic subspace identification for output-only modal analysis. Mech. Syst. Signal Process. 13, 855–878. https://doi.org/10.1006/MSSP.1999.1249.
Pintelon, R., Peeters, B., Guillaume, P., 2010. Continuous-time operational modal analysis in the presence of harmonic disturbances-The multivariate case. Mech. Syst. Signal Process. 24, 90–105. https://doi.org/10.1016/J.YMSSP.2009.03.011.
Ren, X., Xu, Y., Shen, T., Wang, Y., Bhattacharya, S., 2023. Support condition monitoring of monopile-supported offshore wind turbines in layered soil based on model updating. Mar. Struct. 87. https://doi.org/10.1016/j.marstruc.2022.103342.
Röckmann, C., Lagerveld, S., Stavenuiter, J., 2017. Operation and maintenance costs of offshore wind farms and potential multi-use platforms in the Dutch North Sea. Aquaculture perspective of multi-use sites in the open ocean: The untapped potential for marine resources in the anthropocene 97–113.
Shi, X., Williams, M.S., Chatzis, M.N., 2021. A robust algorithm to test the observability of large linear systems with unknown parameters. Mech. Syst. Signal Process. 157. https://doi.org/10.1016/j.ymssp.2021.107633.
Simon, D., 2006. Optimal state estimation: Kalman, H∞, and nonlinear approaches. Optimal State Estimation: Kalman, H∞, and Nonlinear Approaches 1–526. https://doi.org/10.1002/0470045345.
Simpson, H.A., Tatsis, K.E., Abdallah, I., Chatzi, E.N., Chatzis, M.N., 2024. Estimating the foundation parameters of offshore wind turbines through Bayesian model updating. In: Journal of Physics: Conference Series, 112008.
Song, M., Christensen, S., Moaveni, B., Brandt, A., Hines, E., 2022. Joint parameter-input estimation for virtual sensing on an offshore platform using output-only measurements. Mech. Syst. Signal Process. 170, 108814.
Song, M., Mehr, N.P., Moaveni, B., Hines, E., Ebrahimian, H., Bajric, A., 2023. One year monitoring of an offshore wind turbine: variability of modal parameters to ambient and operational conditions. Eng. Struct. 297, 117022.
Stäblein, A.R., Hansen, M.H., Pirrung, G., 2017. Fundamental aeroelastic properties of a bend–twist coupled blade section. J. Fluid Struct. 68. https://doi.org/10.1016/j.jfluidstructs.2016.10.010.
Tatsis, K., Dertimanis, V., Abdallah, I., Chatzi, E., 2017. A substructure approach for fatigue assessment on wind turbine support structures using output-only measurements. In: Procedia Engineering. https://doi.org/10.1016/j.proeng.2017.09.285.
Valikhani, M., Jahangiri, V., Ebrahimian, H., Moaveni, B., Liberatore, S., Hines, E., 2023. Inverse modeling of wind turbine drivetrain from numerical data using Bayesian inference. Renew. Sustain. Energy Rev. 171, 113007. https://doi.org/10.1016/J.RSER.2022.113007.
Valikhani, M., Younesian, D., 2019. Bayesian framework for simultaneous input/state estimation in structural and mechanical systems. Struct. Control Health Monit. 26, e2379.
van der Tempel, J., 2006. Design of Support Structures for Offshore Wind Turbines. TU Delft Repositories [WWW Document]. URL (accessed 7.17.22.
Wang, M., Leng, J., Feng, S., Li, Z., Incecik, A., 2022. Precisely modeling offshore jacket structures considering model parameters uncertainty using Bayesian updating. Ocean Eng. 258. https://doi.org/10.1016/j.oceaneng.2022.111410.
Wei, D., Li, D., Jiang, T., Lyu, P., Song, X., 2023. Load identification of a 2.5 MW wind turbine tower using Kalman filtering techniques and BDS data. Eng. Struct. 281. https://doi.org/10.1016/j.engstruct.2023.115763.
Xu, P., Chen, J., Li, J., Fan, S., Xu, Q., 2023. Using Bayesian updating for monopile offshore wind turbines monitoring. Ocean Eng. 280. https://doi.org/10.1016/j.oceaneng.2023.114801.
Xu, Y., Nikitas, G., Zhang, T., Han, Q., Chryssanthopoulos, M., Bhattacharya, S., Wang, Y., 2020. Support condition monitoring of offshore wind turbines using model updating techniques. Struct. Health Monit. 19, 1017–1031. https://doi.org/10.1177/1475921719875628.
Zou, J., Lourens, E.M., Cicirello, A., 2023. Virtual sensing of subsoil strain response in monopile-based offshore wind turbines via Gaussian process latent force models. Mech. Syst. Signal Process. 200. https://doi.org/10.1016/j.ymssp.2023.110488.